ACS APPLIED MATERIALS & INTERFACES

Research Article

www.acsami.org

Elimination of Burn-in Open-Circuit Voltage Degradation by ZnO Surface Modification in Organic Solar Cells

Zhiming Kam,[†] Xizu Wang,[‡] Jie Zhang,*[,‡] and Jishan Wu*[,†,‡]

[†]Department of Chemistry, National University of Singapore, 3 Science Drive 3, Singapore 117543, Singapore

[‡]Institute of Materials Research and Engineering, A*STAR, 3 Research Link, Singapore 117602, Singapore

Supporting Information

ABSTRACT: Photodegradation of inverted organic solar cells based on ZnO as an electron transport layer (ETL) was studied over short time scales of 5 min and 8 h. Devices with ZnO as ETL reproducibly exhibited a steep loss of open-circuit voltage, V_{OC}, and shunt resistance, R_{SH}, in a matter of minutes upon illumination. Removing the UV-content of illumination minimized V_{OC} loss and impact on the device's shunting behavior, indicating its role in the loss. Application of an ultrathin layer of Al on ZnO led to almost negligible photoinduced V_{OC} loss up to 8 h of exposure. By applying the fundamental Shockley diode equation, we approximated the V_{OC} loss to be caused by dramatic increases in reverse saturation current I_0. We attribute the increased rate of recombination to diminished carrier selectivity at the ZnO/organic interface. Devices with Al modified ZnO ETL demonstrated remarkable R_{SH} (1.4 kΩ cm^2 at 1 sun), rectification ratio (10^6) and reverse saturation current density (2.1×10^{-7} mA/cm^2).

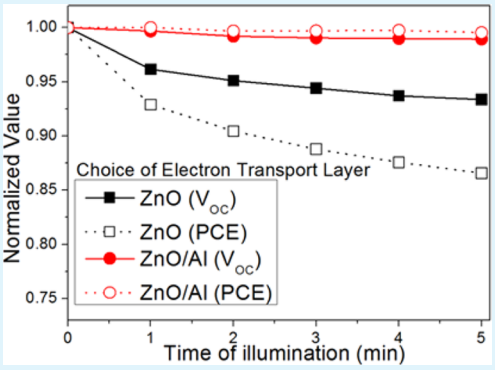

KEYWORDS: *inverted solar cell, P3HT, ZnO, lifetime, degradation*

1. INTRODUCTION

The use of organic photovoltaics (OPV) as a renewable energy source has great promise due to the low monetary and energy costs of production and a potential for lightweight and flexible substrate implementation. High power conversion efficiency (PCE) organic solar cells (OSCs) have traditionally revolved around the use of polymer light absorbing materials in bulk-heterojunction (BHJ) devices, but recently been surpassed by multijunction tandem cells and the use of small molecules, exceeding device conversion efficiencies of 10%.[1−4] Plastic solar cells, as a technology, have thus proven competitive with Si based inorganic solar cells.

However, in order to realize the commercialization of OPV, another important aspect to consider is the reliability, or lifetime, of modules. Problems faced regarding the stability of OSCs include factors such as the chemical[5,6] and photo-instability[7,8] of the light absorbing medium, thermally induced phase changes,[9] interfacial breakdown due to ion-exchange[10] and oxidation[11−13] nonexclusively. To counter some of these issues, the "inverted" geometry in cell architecture was introduced. As opposed to the "conventional" geometry, the cathode is bottom-lying, while the anode is surface facing. This minimizes ambient exposure for the low work-function metal, or excludes altogether the use of such metals, using electron transport layers (ETLs) instead to promote electron extraction.

n-Type metal oxides such as TiO_x and ZnO have seen extensive use in OPV as ETL,[14−17] as well as functioning as recombination layer in tandem cells.[17,18] Besides their application in OPV, both TiO_x and ZnO have also been reported to be used as electron extraction layers in other types of solar cells such as dye-sensitized[19−21] and the more recent perovskite solar cells.[22,23] Devices prepared with ETLs based on TiO_x commonly require an extensive ultraviolet (UV) light-soaking process to "activate", otherwise presenting an S-shape, or inflection, in its current-bias curve.[24] Although the nature of this S-shape is still of debate, the need for extensive UV light-soaking in TiO_x based inverted OSCs is both detrimental to the stability of the organic light absorbing materials and impedes its photovoltaic function. For these reasons the use of ZnO as electron transport layer (ETL) is more desirable.

There are numerous reports of OSCs with ZnO based ETLs demonstrating excellent shelf lifetimes.[17,25] While the shelf stability of ZnO based OSCs are unquestionable, the amount of reports made thus far regarding their operational stability is notably scarce. Careful scrutiny has to be made in this instance, as shelf storage conditions typically involve a lack of both illumination and encapsulation, presenting little information regarding the OSCs' photochemical stability. Both factors are unrealistic: the former contradicts the function of a solar cell, whereas in the latter case, inverted devices have been noted to "self-heal" with the Ag anode oxidizing at the Ag/hole transport layer (HTL) interface and improving hole extracting properties,[26,27] but could be counter-productive if the organic light absorbing layer was exposed similarly to air during operation.

Received: October 13, 2014
Accepted: December 31, 2014
Published: December 31, 2014

DOI: 10.1021/am507056h
ACS Appl. Mater. Interfaces 2015, 7, 1608−1615

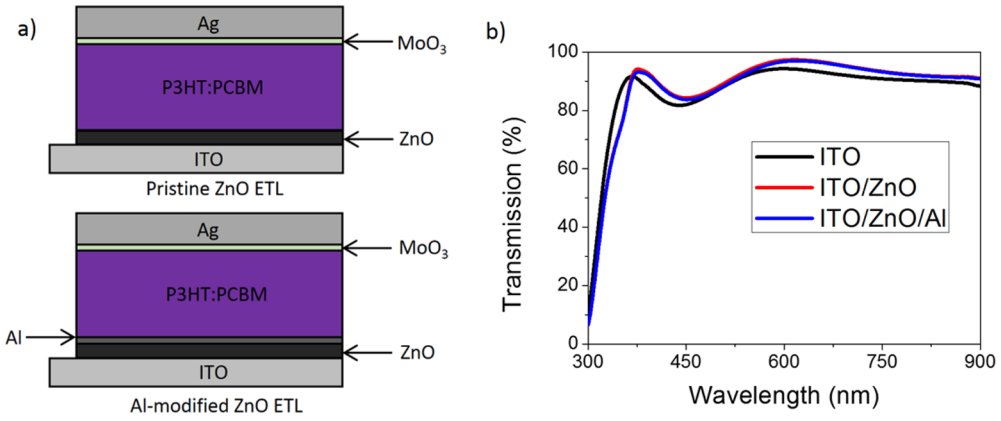

Figure 1. (a) Device architectures of inverted organic solar cells using a ZnO and Al-modified ZnO as electron transport layers, respectively. (b) Optical transmission profiles of ITO, ITO/ZnO and ITO/ZnO/Al electrodes.

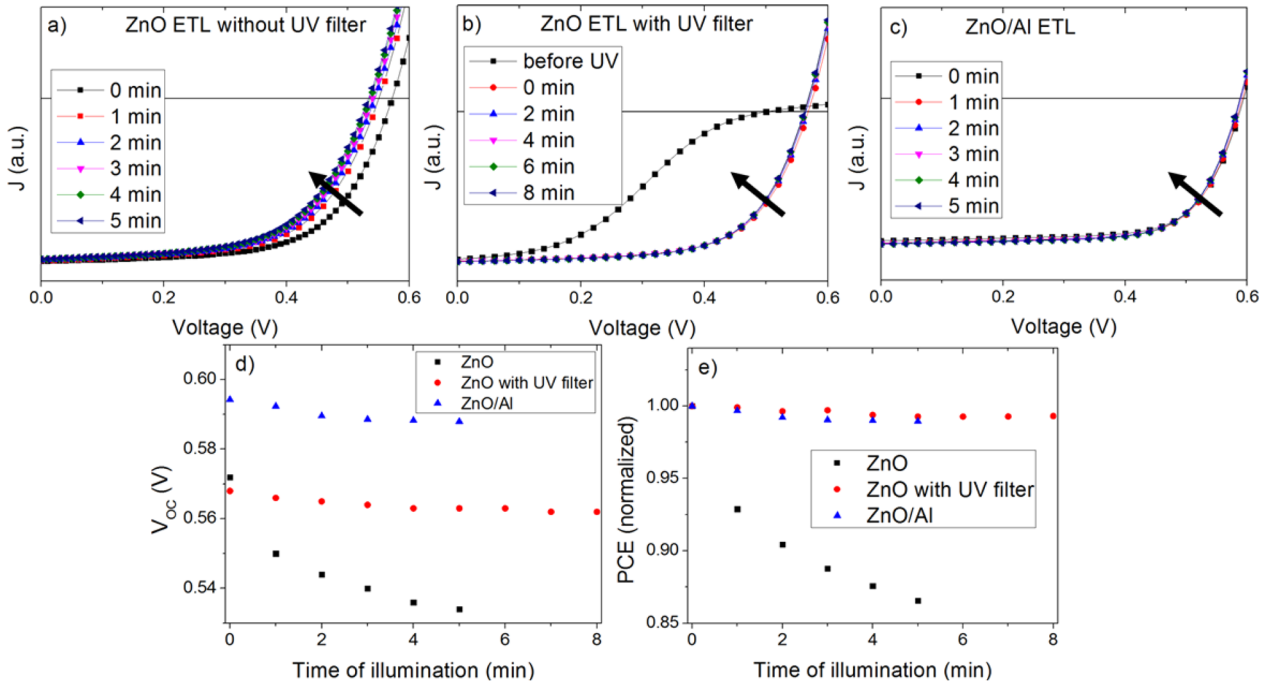

Figure 2. Changes in the current−voltage behavior of devices with (a) ZnO ETL under simulated sunlight for 5 min, (b) ZnO ETL under UV-filtered simulated sunlight for 8 min ("before UV" describes a fresh device prior to any form of light exposure; the device displays inflections similar to devices with unactivated TiO_x layers in literature, "0 min" refers to the device having been briefly exposed to 10s of unfiltered AM1.5G light to active ZnO photoconductivity) and (c) Al-modified ZnO ETL under simulated sunlight for 5 min. Shifts in device (d) V_{OC} and (e) normalized PCE tracked over light exposure duration.

In one example, Manor et al. reported the formation of shunting channels in ZnO at the ZnO/organic interface following photoaging under concentrated simulated sunlight.[28] This was marked by a significant loss of V_{OC}, and a decrease in shunt resistance (R_{SH}). While the article focused on the loss of R_{SH} in correlation with an increase in photoconductivity of the ZnO layer, there was a lack of adequate mention of or explanation for the decrease in V_{OC}. In another instance, Kuwabara et al. also reported on the photoaging of inverted OSCs employing the use of ZnO ETL prepared using different annealing temperatures.[29] Although neither increased shunting nor diminished V_{OC} values were explicitly commented upon, it does indicate that the UV content of simulated sunlight has an important role to play in the photovoltaic performance of these devices.

Considering the importance of ZnO in varied forms of solar cells, both conventional and state-of-the-art, and a distinct shortage of understanding regarding the nature of its impact on the operational lifetime of said devices, we feel that further investigations is due regarding the reported V_{OC} loss in ZnO based inverted OSCs and the role UV-illumination might have to play in it.

In this work, we examine the degradation of inverted OSCs based on a ZnO ETL under operational conditions, both with and without UV content. We show that these devices undergo a significant matter of minutes loss in V_{OC}, the occurrence of which is dependent on the availability of UV light, and attempt to offer an explanation for this phenomenon. By applying a technique we recently demonstrated,[30,31] we simultaneously demonstrate an enhancement in the performance of the device and sequester the substantial V_{OC} loss by modifying the surface

DOI: 10.1021/am507056h
ACS Appl. Mater. Interfaces 2015, 7, 1608−1615

energetic profile of the ZnO ETL by applying an ultrathin layer of Al. We further relate these changes to the concept of charge selectivity at the carrier extracting contacts that has been shown elsewhere to influence the photovoltaic properties of OSCs.[32,33]

2. EXPERIMENTAL SECTION

Device Fabrication. Two types of devices based on the use of a poly(3-hexylthiophene-2,5-diyl):phenyl-C61-butyric acid methyl ester (P3HT:PCBM) BHJ light absorbing layer with an inverted architecture were studied. The two types of devices are inverted OSCs with ZnO ETLs and a variant with the ZnO layer surface modified by the application of an ultrathin layer of metallic Al via thermal evaporation. The structures can be described as glass/ITO/ZnO/P3HT:PCBM/MoO_3/Ag and glass/ITO/ZnO/Al/P3HT:PCBM/MoO_3/Ag respectively (Figure 1a). Optical transmission profiles of the two cathodic arrangements are shown in Figure 1b.

The devices were fabricated on prepatterned ITO glass substrates with sheet resistance of 13−16 Ω/□ that were cleaned by sonication in a sequence of solvents: detergent, deionized water, acetone and isopropyl alcohol. Prior to ZnO layer deposition, the substrates were cleaned by microwave induced argon-sputtering. ZnO was deposited on the substrates by spin coating solutions of ZnO dissolved in NH_3(aq) at 3000 rpm, followed by thermal annealing at 150 °C for 20 min to result in a 15 nm thick ZnO layer. The ZnO-based solution in aqueous NH_3 was prepared as previously described.[34] The organic light absorbing layer was deposited by spin coating a solution of a P3HT (Rieke Metals) and PCBM (Nano-C) blend (20 mg and 16 mg/mL respectively) in dichlorobenzene. The organic layers were left to dry for 2 h before thermally annealed at 140 °C and capped with an anode comprising a MoO_3/Ag bilayer (5 nm, 100 nm) applied via thermal evaporation in vacuo (2×10^{-4} Pa). In the instance of devices with an Al-modified ZnO ETL, a thin layer of Al (1.2 nm) was applied via thermal evaporation in vacuo (2×10^{-4} Pa) prior to the deposition of the organic layer. AFM topographical images of ZnO and Al-modified ZnO films are shown to be relatively similar in surface roughness (Figure S1, Supporting Information).

Device Characterization. The current−voltage characteristics of the devices were measured with a Keithley 2400 SourceMeter under 100 mW/cm^2 (AM 1.5G) simulated sunlight (San-Ei Electronics, XES-70S1). Shadow masks were used to define the active area (0.09 cm^2). Photodegradation of the devices was conducted under modified ISOS-L-1 conditions: the samples were illuminated by the same simulated sunlight source at 1 sun intensity in a glovebox with chemically inert atmosphere (N_2, < 1 ppm of O_2 and H_2O) and under open-circuit conditions. Temperature of the devices were maintained within 25−30 °C by gas cooling during the aging process to minimize thermally induced degradation effects.

3. RESULTS AND DISCUSSION

We first probe the initial photovoltaic performance and subsequent short-term degradation of the described inverted devices under illumination, as summarized in Figure 2. This short-term degradation describes the "burn-in" process in the degradation of a device. Commonly regarded in most lifetime studies as a period of time taken by the OSC to stabilize, this burn-in is often not included in most lifetime studies. However, it is also often responsible for a steep loss in device performances and should be considered if possible to mitigate. Figure 2a shows the evolution of the current density−voltage (J−V) curve of an inverted OSC based on a P3HT:PCBM blend and a ZnO ETL (device A) under continuous simulated sunlight. Device A yields an initial PCE of about 3.2% comparable to literature performances, and displays neither significant inflection point behavior nor shunting reported elsewhere. However, the efficiency of the device rapidly deteriorated to ∼87% of its initial performance after 5 min exposure (Figure 2e). Shifts in its J−V curves attribute this considerable loss in device PCE to a steep decrease of its V_{OC} value from 0.57 to 0.53 V. This change in V_{OC} was tracked over time in Figure 2d. The R_{SH} value approximated from the reciprocal of the zero bias gradient also showed a concurrent decline from about 1.2 to 0.6 kΩ cm^2, indicating an increase in the shunting of photogenerated charges. This agrees with the observation made by Manor et al., albeit not at the same magnitude.[28] On the other hand, minimal changes in short-circuit current density (J_{SC}) were observed due to the short duration of exposure which limits the amount of photobleaching in the organic layer.

Figure 2b shows the J−V curves for a similar ZnO based inverted OSC under illumination, except with UV light content excluded through the application of an UV long-pass filter with a cutoff at 400 nm (device B). A fresh device B with no prior exposure to UV content yielded an inflection around the V_{OC} point. Even after 1 min of UV-filtered AM 1.5G light-soaking, the inflection point did not diminish. However, upon 10 s light-soaking in full AM 1.5G simulated sunlight, the inflection point disappeared (Figure 2b "0 min"). This suggests that small quantities of UV illumination are still necessary for the induction of photoconductivity in the ZnO layer, not unlike extensive light-soaking for TiO_x. Subsequent photoaging of the activated device under UV-filtered simulated sunlight revealed little changes in V_{OC}, as shown in Figure 2d. Unlike in device A, there was negligible change in the shunting behavior of device B under UV-filtered illumination, maintaining a R_{SH} of about 1.3 kΩ cm^2 throughout. To account for the diminished irradiance due to the use of an UV filter, device B was aged for up to 8 min as opposed to 5 min. To put into perspective, the device produced J_{SC} values of 7.1 and 8.1 mA/cm^2 with and without UV filtration, respectively. Comparisons between the J−V characteristics of devices A and B indicate a possibility that UV illumination is entirely responsible for the observed rapid deterioration in V_{OC} and R_{SH}.

To identify whether this UV-induced V_{OC} loss is caused by effects within the organic bulk or at the contact interfaces, the same photoaging process was carried out on a device with a modified ZnO ETL, wherein an ultrathin layer of Al was evaporated onto the surface of the ZnO film (device C). For convenience, we address this ETL as ZnO/Al. However, due to the low reduction potential of Al and the low thickness of the evaporated Al, it is unlikely to remain in elemental form. The ZnO/Al ETL resulted in an enhanced PCE of about 3.3% in device C. This minor improvement can be ascribed to an increase in the initial V_{OC}, from 0.57 to 0.59 V. Similar to previous reports wherein thin layers of Al are evaporated onto metal oxides layers, a decrement in surface work-function is expected following Al oxidation by the ZnO layer, or by ambient oxygen.[30,31,35] We also find that device C exhibits no inflections in its J−V curve prior to UV-exposure, suggesting that the ZnO ETL benefitted from improved electron conductivity from an *n*-doping-like effect from the added Al. In addition to a slight improvement in its photovoltaic performance, the use of a ZnO/Al based ETL in device C appears to render it robust under illumination. When light-soaked for 5 min, no appreciable changes in its J−V characteristics were observed (Figure 2c). The shift in V_{OC} for device C from 5 min light-soaking is minor (6 mV) relative to that for device A (38 mV). Similar to device B, the R_{SH} value under illumination remains unchanged with prolonged illumination, maintaining a value of 1.4 kΩ cm^2. The smaller

DOI: 10.1021/am507056h
ACS Appl. Mater. Interfaces 2015, 7, 1608−1615

shift in V_{OC} and R_{SH} here suggests that the processes linked to the observed photodegradation is primarily located at the ETL/organic interface.

The significance of the burn-in degradation process on the long-term performances of these devices was highlighted by extended photoaging up to 8 h; continued decay in J_{SC}, V_{OC} and PCE parameters were tracked in Figure 3a,b,c, respectively.

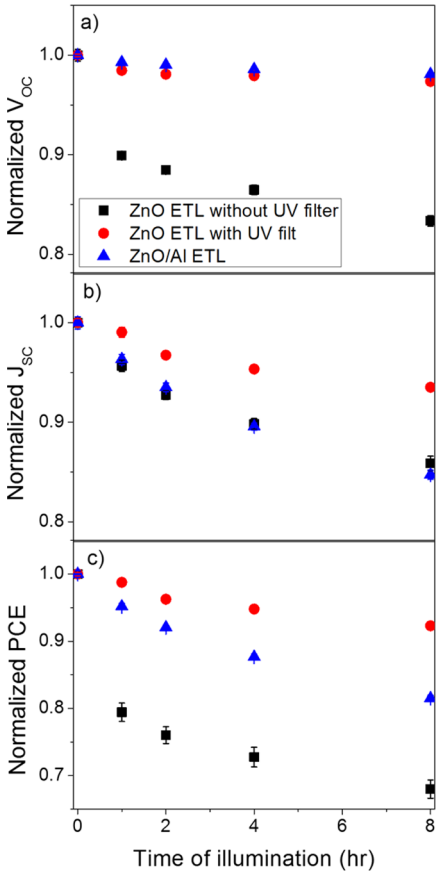

Figure 3. Normalized values of (a) V_{OC}, (b) J_{SC} and (c) PCE tracked over 8 h of photodegradation for devices with variable transport layers and aging conditions. The results were derived from averaging the performances of four diodes for each testing condition.

A 32% and 18% loss in PCE for device A and device C, respectively, can be linked to a decrease in J_{SC}, which appears to be independent of ZnO modification. This damage could be due to either the use of a MoO_3 hole-transport layer or the presence of trace oxygen or moisture in the glovebox as the J_{SC} of inverted OSCs using PEDOT hole-transport layers have been reported as stable under dry nitrogen.[28] Although the reason for this J_{SC} loss is unclear, it does not detract from the obvious point that V_{OC} values for both devices B and C are relatively stable over long-term photoaging, which continued to decay for device A, as demonstrated in Figure 3c.

To explain the initial improvements in photovoltaic performances between devices A and C, we examine the surface energy profile of the two cathodic assemblies, ITO/ZnO and ITO/ZnO/Al, via ultraviolet photoelectron spectroscopy (UPS) using He I excitation energy (21.22 eV), as shown in Figure 4a. The pristine ZnO film prepared by us was determined to have a surface work function of 4.21 eV within the range of previously reported values.[36,37] In comparison, the surface work function of Al-modified ZnO film was calculated to be 3.93 eV. The approximately 0.3 eV reduction in work function between ZnO and ZnO/Al is expected to increase the built-in voltage across the organic bulk in the photodiode, improve the electron extraction properties of the cathode, and thus increase the V_{OC} of the device as observed above. The valence band maximum (VBM) can be additionally determined from the high kinetic energy cutoff of the UPS spectra, and has been detailed in an energy level diagram of the cathode, interlayers, and the organic bulk materials relative to vacuum level in Figure 4b. The VBM for ZnO at the film surface is approximated at 7.1 eV below vacuum level, whereas the VBM for the ZnO/Al surface is at 8.0 eV below vacuum level. In general, a lower work function for the Al-modified ZnO cathode is expected to improve electron extraction kinetics, while the deeper VBM increases hole barrier heights and impedes hole transport across the interface. Overall, the application of an ultrathin Al layer greatly enhances the electron selectivity and hole-blocking properties of the ZnO transport layer. When both types of ETLs have been placed under 10 min of 300 mW/cm^2 UV illumination, we found that their work functions increased by 0.13−0.14 eV similarly. Although this coincides with the general trend of V_{OC} degradation observed in aged devices A and C, the disparity between V_{OC} losses and cathode work function increases for the two devices suggests a loss mechanism besides simply a change in built-in potential.

The relationship between charge selectivity of electrical contacts in solar cells and the observed V_{OC} losses can be

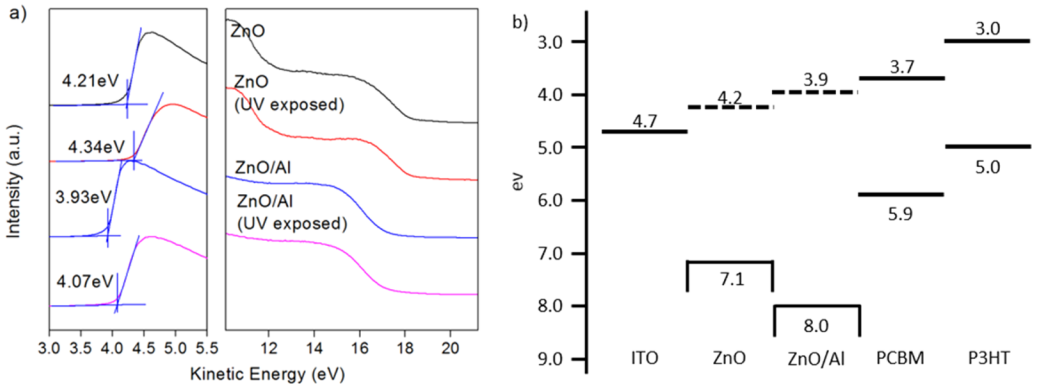

Figure 4. (a) He I UPS spectra of the surface of ITO/ZnO and ITO/ZnO/Al before and after illumination. (b) Approximate energy level diagram of ITO, ZnO, ZnO/Al, PCBM and P3HT.

DOI: 10.1021/am507056h
ACS Appl. Mater. Interfaces 2015, 7, 1608−1615

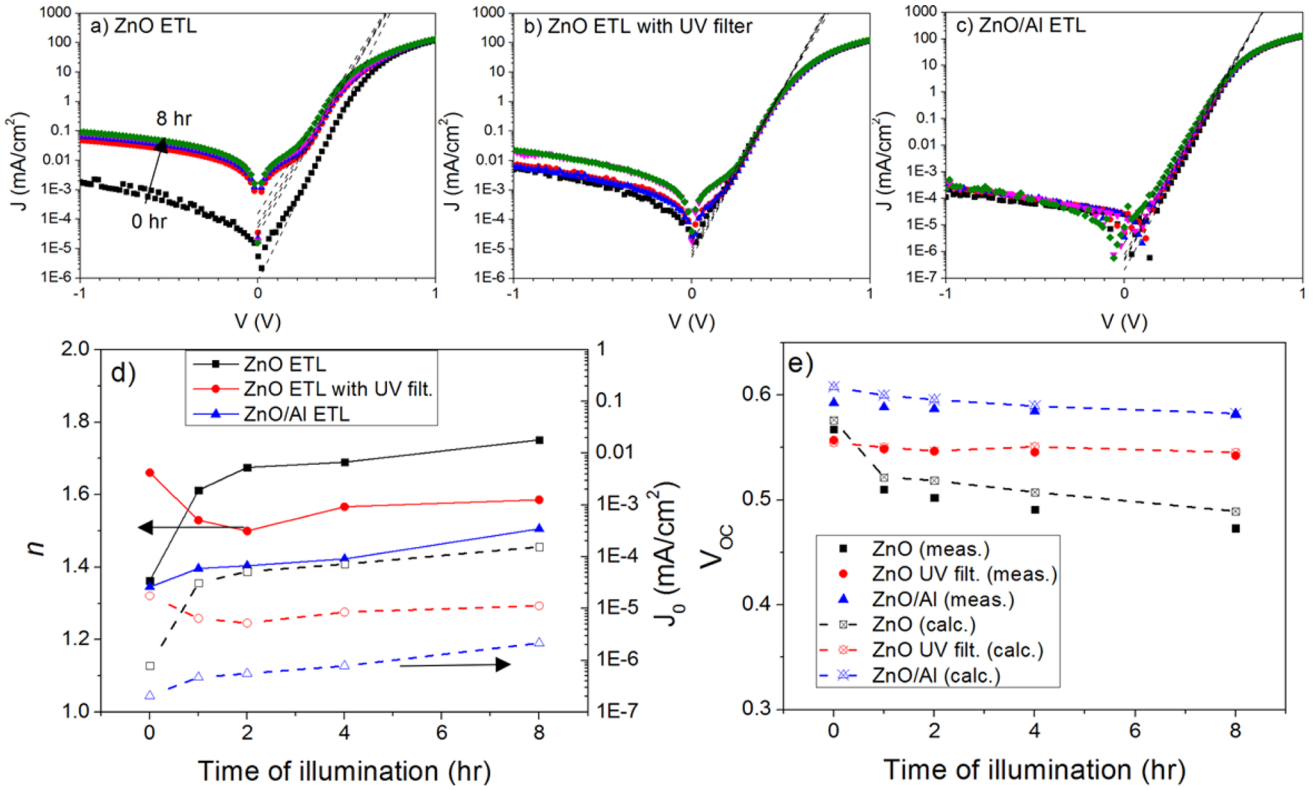

Figure 5. Dark $J-V$ curves of devices with (a) ZnO ETL, (b) ZnO ETL with UV-filtered illumination and (c) Al-modified ZnO ETL at 0, 1, 2, 4 and 8 h of total illumination duration. The dotted lines describe the exponential fit of the dark $J-V$ curves to the Shockley diode approximation of $J = J_0 \exp(qV/nkT)$. (d) Ideality factor n (solid line, solid point) and reverse saturation current density J_0 (dotted line, hollow point) parameters estimated from the dark $J-V$ curves. (e) Approximation of V_{OC} values (dotted line, hollow point) derived from the Shockley diode parameters n and J_0 against experimentally observed V_{OC} (solid point).

understood from assessing their fundamental diode parameters. The Shockley diode equation for a nonideal photodiode is expressed as follows[38]

$$I = I_0\left(\exp\left(\frac{q(V - IR_S)}{nkT}\right) - 1\right) - \frac{V - IR_S}{R_{SH}} + I_{ph} \quad (1)$$

where I describes the diode current, I_0 is the diode reverse saturation current, I_{ph} is photoexcitation current, q is the electron charge, V is the applied bias, R_S and R_{SH} are parasitic series and shunt resistances, n refers to an ideality factor, k the Boltzmann constant and T the temperature in Kelvin. I_0 describes charge recombination of a diode in the dark, and thus implicitly quantifies the leakage of minority carriers due to poorly selective electrical contacts. Consequently, more greatly selective electrical contacts would result in lower I_0 and the converse is expected to be true. For greater clarity, a selective contact can be defined as one which preferentially extracts majority carriers and blocks both collection and injection of minority carriers via high energy barriers.[32]

By approximating negligible R_S and infinite R_{SH}, fitting of the natural logarithm of I against V under dark conditions and intermediate bias allows for the estimation of both n and I_0 (eq 2).

$$\ln I \approx \ln I_0 + \frac{qV}{nkT} \quad (2)$$

Manipulation of eq 1 under open-circuit conditions ($I_{ph} = -I_{SC}$, $I = 0$, $V = V_{OC}$) and assuming minimal resistive losses ($R_{SH} \gg R_S$, $R_S \approx 0$) yields the following relationship:

$$V_{OC} \approx \frac{nkT}{q}\ln\left(\frac{I_{SC}}{I_0} + 1\right) \quad (3)$$

Equation 3 indicates that the V_{OC} of a photodiode in operation is governed mainly by n and I_0. By estimating these parameters via eq 2, we can attempt to explain the observed V_{OC} loss.

The dark $J-V$ curves of devices A, B and C presented in Figure 5a–c illustrate the evolution of their dark diode characteristics with light exposure up to 8 h. The immediate observation here is a precipitous drop in the rectification ratio ($\pm$1.0 V) of device A within the first hour from 6.7×10^4 to 2.8×10^3, which then further decreases to 1.5×10^3 at 8 h. This loss in rectifying behavior reflects the previously mentioned decrease in R_{SH}, and is attributed to a degradation of the minority carrier barriers at the electrical contacts. This is expected as reverse current for a photodiode in the dark is dominated by the injection of minority carriers. Despite presenting a lower initial ratio of 2.2×10^4, device B retained its rectifying behavior in the absence of UV illumination. The lower initial rectification ratio in device B is possibly due to shunting from preparation defects such as ZnO roughness, whereas the magnitude of the later decrement of the ratio due to photodegradation is of greater significance as an indication of diminished charge selectivity at the charge extracting contacts. The high initial rectification ratio observed in device C (1.2×10^6), which dropped slightly (5.8×10^5) after 8 h of light exposure, implies that the reduced selectivity of transport layers observed in device A occurred at least in part at the ZnO/organic interface, and that the Al modification provides a photostable enhancement in its the hole blocking capacity.

DOI: 10.1021/am507056h
ACS Appl. Mater. Interfaces 2015, 7, 1608–1615

Exponential fitting was conducted on each curve in Figure 5a–c; their respective n and I_0 values have been detailed in Figure 5d. A temperature of 300 K was assumed, and the fitting was carried out within a 0.3–0.5 V range to minimize errors in estimation due to the voltage dependence of the ideality factor. The estimation shows that both devices A and C possess an initial n value close to 1.35. In the case of device A, n rapidly increased to 1.61 after 1 h, followed by a slow rise to 1.75 at 8 h of light exposure. On the other hand, device C experienced a gradual increase in n to 1.50 after the same duration. Equation 3 predicts that the n value alone would incur an increase in the V_{OC} values of these devices. However, these shifts in n were mitigated by a simultaneous increase in their reverse saturation current I_0, which was much larger for device A (7.9×10^{-7} to 1.6×10^{-4} mA/cm^2) than device C (2.1×10^{-7} to 2.2×10^{-6} mA/cm^2). The overall effect for device A is a greatly diminished V_{OC} from its original value, whereas device C underwent a much smaller loss. Unlike device A, device B experienced slight reductions in its n and I_0 values after 8 h UV-filtered illumination. Figure 5e shows the V_{OC} predicted by eq 3 in comparison with measured V_{OC} values; the estimated values and trends agree with the experimentally determined values, verifying the validity of the estimated n and I_0 values.

The ideality factor n reflects the mode of charge recombination in a diode. Specifically, when n is unity, the diode is ideal and charge recombination occurs mainly via a band-to-band pathway. However, when n approaches a value of 2,[39−41] charge recombination in a diode is dominated either by a Shockley–Read–Hall (trap-assisted) recombination process[42] or recombination in the depletion region of a junction.[43] For the purpose of this study, we consider the two equivalent as minority carriers in a space charge region are effectively confined by high potential barriers. Therefore, increments in the ideality factors of devices A and C can be interpreted as a shift in the recombination mode of the photodiodes toward a trap-assisted process. Since devices A and C are architecturally similar except for a surface Al-modification of ZnO, we conclude that this trap-assisted recombination occurs due to degradation in the hole blocking contact.

The deep valence band edge of ZnO (7.1 eV below vacuum level) efficiently blocks hole transport across the ZnO ETL and charge recombination under low forward and reverse bias is normally expected to be limited. However, in the case of device A we find that illumination under simulated sunlight with UV content heavily increases the reverse saturation current from charge recombination. Under low forward bias, comparisons with device C indicate there is a significant diffusion of holes from the organic bulk layer across the ZnO layer into ITO. The corresponding effective barrier height Φ_B for current leakage across the devices can be determined from J_0 according to eq 4 based on thermionic emission theory:[44,45]

$$J_0 = A^* T^2 \exp\left(\frac{-q\Phi_B}{kT}\right) \quad (4)$$

where A^* refers to a material specific Richardson constant. By assuming A^* to be 10.41 A/cm^2 K^2 for P3HT:PCBM from literature,[46] the Φ_B values for devices A, B and C were estimated and charted against duration of light exposure (Figure S2, Supporting Information). The changes in V_{OC} with illumination for devices A and C are more coherent with changes in their Φ_B than cathode work function, indicating that the degradation described in this work is predominantly due to diminished hole barrier height across the ZnO ETL. We thus deduce that UV light erodes the hole blocking capacity of ZnO and so reduces its overall charge selectivity. Device B, in the absence of UV, experienced no similar compromise in the charge selectivity of its contacts. Φ_B for device C is reduced after 8 h of photoaging but remained significantly higher than that for device A, thus maintaining greater charge selectivity.

To explain the reduction in charge selectivity for ZnO due to UV illumination in device A, we propose the following mechanism (Figure S3, Supporting Information): a fresh ZnO layer by default has a high defect density, introducing states in its forbidden band that acts as both electron traps and hole traps. The presence of electron traps limits its conductivity expressed in the form of inflection on its J–V curve (Figure 2b). High frequency illumination such as UV causes photoexcitation in the ZnO layer via promotion of electrons into the conduction band and leaving holes in the valence band. The valence band edge of ZnO is low and efficiently blocks both hole injection from ITO and extraction from the organic bulk layer. This photoinduced conductivity in ZnO is persistent (Figure 2b) and can last for days.[47] This was explained as the localized capturing of photogenerated holes by deep hole traps as calculated by Zhang et al.[48] Extensive UV illumination leads to the accumulation of both free electrons and deeply trapped holes in the ZnO layer. When the density of trapped holes is sufficiently high, there is the potential for the hopping transport of holes across the ETL. In reverse bias, this means injection of holes from ITO into the organic bulk layer. This is consistent with an increase in I_0, reductions in R_{SH} and hole barrier height inferred from Φ_B (Figure S2, Supporting Information). Another consequence of hole accumulation is the provision of trap-assisted recombination sites for electrons from PCBM at ZnO/organic interface. This explains the deviation from ideal diode recombination marked by an increase in n observed experimentally previously (Figure 5d). Simultaneously, the abundance of electrons in the ZnO conduction band eases recombination with holes from P3HT at ZnO/organic interface. Because the V_{OC} of a device under illumination is determined by a competition between charge generation (I_{SC}) and recombination (I_0), as described by eq 3, the net effect is a V_{OC} loss. By applying an ultrathin layer of Al onto the ZnO surface, a reduction in surface work function is induced as observed in Figure 4. The resultant shift of the Fermi level toward the conduction band increases free electron density at the ZnO surface, granting it high charge conductivity even in the absence of UV illumination.[49] Additionally, the low work function moderates the space charge region of ZnO at the ETL/organic interface negatively. An effect of this moderation, coupled with a deeper VBM, is an increase in hole barrier height, which is expected to increase the overall selectivity of the ZnO/Al transport layer and suppress the reverse saturation current.

4. CONCLUSION

In summary, we have shown OSCs based on an ITO/ZnO/P3HT:PCBM/MoO_3/Ag sandwich to be sensitive to the amount of UV illumination it is exposed to. The ZnO ETL was shown to require a minute amount of UV light to bring about significant and persistent photoconductivity. Unfortunately, extensive exposure to UV light has a deleterious effect in these devices, lowering the effective V_{OC} rapidly in a matter of minutes from 0.57 to 0.53 V. Devices aged under UV-filtered illumination, however, show little degradation. By modifying

DOI: 10.1021/am507056h
ACS Appl. Mater. Interfaces 2015, 7, 1608–1615

the surface of the ZnO ETL with an ultrathin layer of Al, improved efficiencies due to enhanced V_{OC} of 0.59 V, and photostability under simulated sunlight were observed. Continuous photoaging for 8 h shows that V_{OC} losses accumulate for ZnO based devices, whereas neither of the other two devices exhibit significant V_{OC} degradation. UPS measurements suggest that the observed improvements in the ZnO/Al based device to be due to lowered work function and deeper VBM. Dark $J-V$ curves of these devices were examined by Shockley diode equation parameters such as ideality factor and reverse saturation current. The diode parameters suggest the ZnO based device experienced a dramatic increase in its reverse saturation current upon illumination due to a decrease in barrier height, causing the severe V_{OC} loss observed. We associate the degradation to a reduction in the hole blocking capacity of the ZnO ETL caused by UV light. The device with the Al modified ZnO ETL experienced much less changes in its photovoltaic and diode parameters prior and post photoaging due to its already lower surface work function and deeper VBM.

■ ASSOCIATED CONTENT

Ⓢ Supporting Information

Surface topography of ZnO and ZnO/Al films via AFM, table summarizing changes in photovoltaic parameters of devices A-C before and after 8 h illuminationband diagrams describing the proposed degradation mechanism of ZnO with UV illumination, changes in the calculated Φ_B of devices A−C against illumination duration, and band diagrams describing the proposed degradation mechanism of ZnO with UV illumination. This material is available free of charge via the Internet at http://pubs.acs.org.

■ AUTHOR INFORMATION

Corresponding Authors

*J. Wu. E-mail: chmwuj@nus.edu.sg.
*J. Zhang. E-mail: zhangj@imre.a-star.edu.sg.

Author Contributions

The paper was written through contributions of all authors. All authors have given approval to the final version of the paper.

Notes

The authors declare no competing financial interest.

■ ACKNOWLEDGMENTS

The authors thank the financial support from A*STAR SERC Printed Electronics Program (Grant #1021700134 and #1021700137).

■ REFERENCES

(1) You, J.; Chen, C.-C.; Hong, Z.; Yoshimura, K.; Ohya, K.; Xu, R.; Ye, S.; Gao, J.; Li, G.; Yang, Y. 10.2% Power Conversion Efficiency Polymer Tandem Solar Cells Consisting of Two Identical Sub-Cells. *Adv. Mater.* **2013**, *25*, 3973−3978.

(2) Liu, Y.; Chen, C.-C.; Hong, Z.; Gao, J.; Yang, Y. (M.; Zhou, H.; Dou, L.; Li, G.; Yang, Y. Solution-Processed Small-Molecule Solar Cells: Breaking the 10% Power Conversion Efficiency. *Sci. Rep.* **2013**, *3*, 3356.

(3) You, J.; Dou, L.; Yoshimura, K.; Kato, T.; Ohya, K.; Moriarty, T.; Emery, K.; Chen, C.-C.; Gao, J.; Li, G.; Yang, Y. A Polymer Tandem Solar Cell with 10.6% Power Conversion Efficiency. *Nat. Commun.* **2013**, *4*, 1446.

(4) Service, R. Outlook Brightens for Plastic Solar Cells. *Science* **2011**, *332*, 293.

(5) Norrman, K.; Krebs, F. C. Lifetimes of Organic Photovoltaics: Using TOF-SIMS and $^{18}O_2$ Isotopic Labelling to Characterise Chemical Degradation Mechanisms. *Sol. Energy Mater. Sol. Cells* **2006**, *90*, 213−227.

(6) Norrman, K.; Larsen, N. B.; Krebs, F. C. Lifetimes of Organic Photovoltaics: Combining Chemical and Physical Characterisation Techniques to Study Degradation Mechanisms. *Sol. Energy Mater. Sol. Cells* **2006**, *90*, 2793−2814.

(7) Tournebize, A.; Bussière, P.-O.; Rivaton, A.; Gardette, J.-L.; Medlej, H.; Hiorns, R. C.; Dagron-Lartigau, C.; Krebs, F. C.; Norrman, K. New Insights into the Mechanisms of Photodegradation/Stabilization of P3HT:PCBM Active Layers Using Poly(3-hexyl-d_{13}-Thiophene). *Chem. Mater.* **2013**, *25*, 4522−4528.

(8) Sai, N.; Leung, K.; Zádor, J.; Henkelman, G. First Principles Study of Photo-Oxidation Degradation Mechanisms in P3HT for Organic Solar Cells. *Phys. Chem. Chem. Phys.* **2014**, *16*, 8092−8099.

(9) Zhao, J.; Sweinnen, A.; Assche, G. V.; Manca, J.; Vanderzande, D.; Mele, B. V. Phase Diagram of P3HT/PCBM Blends and Its Implication for the Stability of Morphology. *J. Phys. Chem. B* **2009**, *113*, 1587−1591.

(10) deJong, M. P.; van IJzendoorn, L. J.; de Voigt, M. J. A. Stability of the Interface between Indium−Tin−Oxide and Poly(3;4-ethylenedioxythiophene)/Poly(styrenesulfonate) in Polymer Light-Emitting Diodes. *Appl. Phys. Lett.* **2000**, *77*, 2255−2257.

(11) Paci, B.; Generosi, A.; Rossi Albertini, V.; Perfetti, P.; de Bettignies, R.; Sentein, C. Time-Resolved Morphological Study of Organic Thin Film Solar Cells Based on Calcium/Aluminium Cathode Material. *Chem. Phys. Lett.* **2008**, *461*, 77−81.

(12) Cros, S.; Firon, M.; lenfant, S.; Trouslard, P.; Beck, L. Study of Thin Calcium Electrode Degradation by Ion Beam Analysis. *Nucl. Instrum. Methods Phys. Res., Sect. B* **2008**, *251*, 257−260.

(13) Jørgensen, M.; Norrman, K.; Krebs, F. C. Stability/Degradation of Polymer Solar Cells. *Sol. Energy Mater. Sol. Cells* **2008**, *92*, 686−714.

(14) Tao, C.; Ruan, S. P.; Zhang, X. D.; Xie, G. H.; Shen, L.; Kong, X. Z.; Dong, W.; Liu, C. X.; Chen, W. Y. Performance Improvement of Inverted Solar Cells with Different Top Electrodes by Introducing a MoO_3 Buffer Layer. *Appl. Phys. Lett.* **2008**, *93*, 193307.

(15) Hau, S. K.; Yip, H. L.; Baek, N. S.; Zou, J. Y.; O'Malley, K.; Jen, A. K. Y. Air-Stable Inverted Flexible Polymer Solar Cells Using Zinc Oxide Nanoparticles as an Electron Selective Layer. *Appl. Phys. Lett.* **2008**, *92*, 253301.

(16) Hau, S. K.; Yip, H. L.; Ma, H.; Jen, A. K. Y. High Performance Ambient Processed Inverted Polymer Solar Cells through Interfacial Modification with a Fullerene Self-Assembled Monolayer. *Appl. Phys. Lett.* **2008**, *93*, 233304.

(17) Kyaw, A. K. K.; Sun, X. W.; Jiang, C. Y.; Lo, G. Q.; Zhao, D. W.; Kwong, D. L. An Inverted Organic Solar Cell Employing a Sol−Gel Derived ZnO Electron Selective Layer and Thermal Evaporated MoO_3 Hole Selective Layer. *Appl. Phys. Lett.* **2008**, *93*, 221107.

(18) Kim, J. Y.; Lee, K.; Coates, N. E.; Moses, D.; Nguyen, T.-Q.; Dante, M.; Heeger, A. J. Efficient Tandem Polymer Solar Cells Fabricated by All-Solution Processing. *Science* **2007**, *317*, 222−225.

(19) Law, M.; Greene, L. E.; Johnson, J. C.; Saykally, R.; Yang, P. Nanowire Dye-Sensitized Solar Cells. *Nat. Mater.* **2005**, *4*, 455−459.

(20) Zhang, Q.; Dandeneau, C. S.; Zhou, X.; Cao, G. ZnO Nanostructures for Dye-Sensitized Solar Cells. *Adv. Mater.* **2009**, *21*, 4087−4108.

(21) Bach, U.; Lupo, D.; Comte, P.; Moser, J. E.; Weissörtel, F.; Salbeck, J.; Spreitzer, H.; Grätzel, M. Solid-State Dye-Sensitized Mesoporous TiO_2 Solar Cells with High Photon-to-Electron Conversion Efficiencies. *Nature* **1998**, *395*, 583−585.

(22) You, J.; Hong, Z.; Yang, Y. (M.); Chen, Q.; Cai, M.; Song, T.-B.; Chen, C.-C.; Lu, S.; Liu, Y.; Zhou, H.; Yang, Y. Low-Temperature Solution-Processed Perovskite Solar Cells with High Efficiency and Flexibility. *ACS Nano* **2014**, *8*, 1674−1680.

(23) Liu, D.; Kelly, T. L. Perovskite Solar Cells with a Planar Heterojunction Structure Prepared using Room-Temperature Solution Processing Techniques. *Nat. Photonics* **2014**, *8*, 133−138.

DOI: 10.1021/am507056h
ACS Appl. Mater. Interfaces 2015, 7, 1608−1615

(24) Kuwabara, T.; Nakayama, T.; Uozuimi, K.; Yamaguchi, T.; Takahashi, K. Highly Durable Inverted-Type Organic Solar Cell using Amorphous Titanium Oxide as Electron Collection Electrode Inserted between ITO and Organic Layer. *Sol. Energy Mater. Sol. Cells* **2008**, *92*, 1476−1482.
(25) You, J.; Chen, C.-C.; Dou, L.; Muras, S.; Duan, H.-S.; Hawks, S. A.; Xu, T.; Son, H. J.; Yu, L.; Li, G.; Yang, Y. Metal oxide Nanoparticles as an Electron-Transport Layer in High-Performance and Stable Inverted Polymer Solar Cells. *Adv. Mater.* **2012**, *24*, 5267−5272.
(26) Lloyd, M. T.; Peters, C. H.; Garcia, A.; Kauvar, I. V.; Berry, J. J.; Reese, M. O.; McGehee, M. D.; Ginley, D. S.; Olson, D. C. Influence of the Hole-Transport Layer on the Initial Behavior and Lifetime of Inverted Organic Photovoltaics. *Sol. Energy Mater. Sol. Cells* **2011**, *95*, 1382−1388.
(27) Kim, J. B.; Kim, C. S.; Kim, Y. S.; Loo, Y. L. Oxidation of Silver Electrodes Induces Transition from Conventional to Inverted Photovoltaic Characteristics in Polymer Solar Cells. *Appl. Phys. Lett.* **2009**, *95*, 183301.
(28) Manor, A.; Katz, E. A.; Tromholt, T.; Krebs, F. C. Electrical and Photo-Induced Degradation of ZnO Layers in Organic Photovoltaics. *Adv. Energy Mater.* **2011**, *1*, 836−843.
(29) Kuwabara, T.; Tamai, C.; Omura, Y.; Yamaguchi, T.; Taima, T.; Takahasi, K. Effect of UV Light Irradiation on Photovoltaic Characteristics of Inverted Polymer Solar Cells Containing Sol-Gel Zinc Oxide Electron Collection Layer. *Org. Electronics* **2013**, *14*, 649−656.
(30) Kam, Z.; Yang, Q.; Wang, X.; Wu, B.; Zhu, F.; Zhang, J.; Wu, J. Enhanced Absorbance and Electron Collection in Inverted Organic Solar Cells: Optical Admittance and Transient Photocurrent Analyses. *Org. Electron.* **2014**, *15*, 1306−1311.
(31) Chang, J.; Kam, Z.; Lin, Z.; Zhu, C.; Zhang, J.; Wu, J. TiOx/Al Bilayer as Cathode Buffer Layer for Inverted Organic Solar Cell. *Appl. Phys. Lett.* **2013**, *103*, 173303.
(32) Ratcliff, E. L.; Garcia, A.; Paniagua, S. A.; Cowan, S. R.; Giordano, A. J.; Ginley, D. S.; Marder, S. R.; Berry, J. J.; Olson, D. C. Investigating the Influence of Interfacial Contact Properties on Open Circuit Voltages in Organic Photovoltaic Performance: Work Function versus Selectivity. *Adv. Energy Mater.* **2013**, *3*, 647−656.
(33) Guerrero, A.; Dörling, B.; Ripolles-Sanchis, T.; Aghamohammadi, M.; Barrena, E.; Campoy-Quiles, M.; Garcia-Belmonte, G. Interplay between Fullerene Surface Coverage and Contact Selectivity of Cathode Interfaces in Organic Solar Cells. *ACS Nano* **2013**, *7*, 4637−4646.
(34) Wei, W.; Zhang, C.; Chen, D.; Wang, Z.; Zhu, C.; Zhang, J.; Lu, X.; Hao, Y. Efficient "Light-soaking"-free Inverted Organic Solar Cells with Aqueous Solution Processed Low-Temperature ZnO Electron Extraction Layers. *ACS Appl. Mater. Interfaces* **2013**, *5*, 13318−13324.
(35) Gabas, M.; Gota, S.; Ramos-Barrado, J. R.; Sanchez, M.; Barrett, N. T.; Avila, J.; Sacchi, M. Unraveling the Conduction Mechanism of Al-Doped ZnO films by Valence Band Soft X-ray Photoemission Spectroscopy. *Appl. Phys. Lett.* **2005**, *86*, 042104.
(36) White, M. S.; Olson, D. C.; Shaheen, S. E.; Kopidakis, N.; Ginley, D. S. Inverted Bulk-Heterojunction Organic Photovoltaic Device Using a Solution-Derived ZnO Underlayer. *Appl. Phys. Lett.* **2006**, *89*, 143517.
(37) Davis, R. J.; Lloyd, M. T.; Ferreira, S. R.; Bruzek, M. J.; Watkins, S. E.; Lindell, L.; Sehati, P.; Fahlman, M.; Anthony, J. E.; Hsu, J. W. P. Determination of Energy Level Alignment at Interfaces of Hybrid and Organic Solar Cells under Ambient Environment. *J. Mater. Chem.* **2011**, *21*, 1721−1729.
(38) Kippelen, B.; Brédas, J.-L. Organic Photovoltaics. *Energy Environ. Sci.* **2009**, *2*, 251−261.
(39) Leong, W. L.; Cowan, S. R.; Heeger, A. J. Differential Resistance Analysis of Charge Carrier Losses in Organic Bulk Heterojunction Solar Cells: Observing the Transition from Bimolecular to Trap-Assisted Recombination and Quantifying the Order of Recombination. *Adv. Energy Mater.* **2011**, *1*, 517−522.
(40) Street, R. A.; Schoendorf, M. Interface State Recombination in Organic Solar Cells. *Phys. Rev. B* **2010**, *81*, 205307.
(41) Kirchartz, T.; Pieters, B. E.; Kirkpatrick, J.; Rau, U.; Nelson, J. Recombination via Tail States in Polythiophene:Fullerene Solar Cells. *Phys. Rev. B* **2011**, *83*, 115209.
(42) Shockley, W.; Read, W. T., Jr. Statistics of the Recombination of Holes and Electrons. *Phys. Rev.* **1952**, *87*, 835−842.
(43) Sah, C. T.; Noyce, R. N.; Shockley, W. Carrier Generation and Recombination in p-n Junctions and p-n Junction Characteristics. *Proc. IRE* **1957**, *45*, 1228.
(44) Crowell, C. R. The Richardson Constant for Thermionic Emission in Schottky Barrier Diodes. *Solid-State Electron.* **1965**, *8*, 395−399.
(45) He, C.; Zhong, C.; Wu, H.; Yang, R.; Yang, W.; Huang, F.; Bazan, G. C.; Cao, Y. Origin of the Enhanced Open-Circuit Voltage in Polymer Solar Cells via Interfacial Modification Using Conjugated Polyelectrolyes. *J. Mater. Chem.* **2010**, *20*, 2617−2622.
(46) Yakuphanoglu, F.; Anand, R. S. Charge Transport Properties of an Organic Solar Cell. *Synth. Met.* **2010**, *160*, 2250−2254.
(47) Studenikin, S. A.; Golego, N.; Cocivera, M. Optical and Electrical Properties of Undoped ZnO Films Grown by Spray Pyrolysis of Zinc Nitrate Solution. *J. Appl. Phys.* **1998**, *83*, 2104.
(48) Zhang, S. B.; Wei, S.-H.; Zunger, A. Intrinsic *n*-type versus *p*-type Doping Asymmetry and the Defect Physics of ZnO. *Phys. Rev. B* **2001**, *63*, 075205.
(49) Experimentally determined by measuring the dark J-V curve of fresh device C prior to any form of illumination. The higher forward current compared to device B under the same circumstances indicate higher charge conductivity.

DOI: 10.1021/am507056h
ACS Appl. Mater. Interfaces 2015, 7, 1608−1615